

Open quantum spin chains with non-reciprocity: a theoretical approach based on the time-dependent generalized Gibbs ensemble

Alice Marché ^{1*}, Hironobu Yoshida ², Alberto Nardin ¹, Hosho Katsura ^{2,3,4},
Leonardo Mazza ^{1,5}

1 Université Paris-Saclay, CNRS, LPTMS, 91405, Orsay, France

2 Department of Physics, Graduate School of Science, The University of Tokyo, 7-3-1
Hongo, Tokyo 113-0033, Japan

3 Institute for Physics of Intelligence, The University of Tokyo, 7-3-1 Hongo, Tokyo
113-0033, Japan

4 Trans-scale Quantum Science Institute, The University of Tokyo, 7-3-1, Hongo, Tokyo
113-0033, Japan

5 Institut Universitaire de France, 75005, Paris, France

* alice.marche@universite-paris-saclay.fr

January 14, 2026

Abstract

We study an open quantum spin chain with non-reciprocal dissipation using a theoretical approach known as time-dependent generalized Gibbs ensemble. In the regime of weak dissipation the system is fully characterized by its rapidity distribution and we derive a closed set of coupled differential equations governing their time evolution. We check the accuracy of this theory by benchmarking the results against numerical simulations. Using this framework we are able to compute both the magnetization density and current dynamics, identifying some relations between the two. The problem of the anomalous power-law exponents identified in a previous work is discussed. Our work constitutes a theoretical approach that is able to describe the physics of non-reciprocal open quantum spin chains beyond analyses based on non-interacting fermions.

Contents

1 Introduction	2
2 Model and known results	4
2.1 The model	4
2.2 Known results on the algebraic decay of the magnetization	4
2.3 Free fermions	5
3 Time-dependent generalized Gibbs ensemble (t-GGE)	7
3.1 t-GEE for the spin model in Eqs. (1) on an infinite lattice	7
3.2 Equation of motion for the rapidity distribution	8
3.3 The time-evolving rapidity distribution	9
4 Time decay of the magnetization	10

4.1	Comparison between the t-GGE results and tensor-network simulations	10
4.2	Late-time decay	11
5	Hamiltonian magnetization current	14
6	Conclusion and perspectives	14
A	Proof that $\langle c^\dagger(k)c(q) \rangle = 0$ for $k \neq q$	16
B	Derivation of Eq. (9)	16
C	Derivation of Eq. (12)	17
D	Derivation of Eq. (20)	18
E	Details on the numerical solution of Eq. (21)	20
F	Details on the finite size numerical computation via quantum trajectories	20
References		21

1 Introduction

In the classical world, out-of-equilibrium many-body systems often exhibit non-reciprocal interactions among their elementary constituents: the action-reaction symmetry is broken whenever one component can influence another without being affected in the same way. Biological systems characterised by predator-prey interactions are a paradigmatic example, nowadays falling into the broad class of living active matter [1–3]; recently, also synthetic systems have shown this behaviour [4,5]. Peculiar out-of-equilibrium phenomenology without a counterpart in equilibrium systems [6,7] has been identified, including spontaneous directed motion without external bias [8], odd elastic and transport responses [9], and unusual collective modes that violate standard fluctuation-dissipation relations [10].

Motivated by these results, the question of whether non-reciprocal quantum systems can be engineered has attracted significant attention. Early studies of quantum non-reciprocity typically postulated a non-Hermitian Hamiltonian, which can arise from post-processing a measured quantum system, or from a suitable integration of the environment [11]. In this respect, the Hatano-Nelson model is a paradigmatic example, showcasing remarkable phenomena, such as the non-Hermitian skin effect, a strong spectral sensitivity on the boundary conditions, and non-reciprocal transport [12–15].

More recently, it has been proposed to study non-reciprocal interactions using a Lindblad master equation [16–18], which describes quantum systems weakly-coupled to a Markovian environment [19]. The main experimental proposal for realizing a non-reciprocal open quantum spin chain relies on two key aspects: (i) the breaking of time-reversal symmetry, and (ii) the presence of dissipation; the interplay between these ingredients enables asymmetric couplings between quantum degrees of freedom [16–18]. In practice, one considers a nearest-neighbour Hamiltonian with synthetic gauge fields which break time-reversal invariance, while coupling neighbouring lattice sites to the same dissipative reservoir; the setup is then effectively described by a Lindblad master equation featur-

ing two-site and spatially-directed jump operators. The relation of these setups to the Hatano-Nelson non-Hermitian Hamiltonian, and the many similarities between the two, have been discussed [20].

This proposal has attracted a lot of interest and the model has been subsequently thoroughly investigated, focusing on the original bosonic formulation motivated by photonics, but also extending it to quantum spin chains and fermionic systems. The appearance of persistent currents induced solely by reservoir engineering has been clearly demonstrated [21]. In the presence of hard-wall boundary conditions, the setup displays eigenstates that are exponentially localized at the edges, a manifestation of the non-Hermitian skin effect [22]. This phenomenology has also been employed to discuss directional amplification in non-reciprocal open quantum systems [23–25]. The existence of repulsively-bound doublon quasiparticles in a bosonic setting motivated by quantum-optics applications, which are bound together by interactions, and their non-reciprocal dynamics, has been shown in Ref. [26].

Other works have specifically focused on the emergence of universal critical behaviors in the late-time algebraic decay $\sim t^{-\chi}$ of an observable associated with the closure of the Lindbladian spectral gap in the thermodynamic limit [27–29]. Different power law exponents χ have been found depending on whether one considers (i) a fermionic system, focusing on the fermionic number, or (ii) a spin system, discussing the magnetization. In the case (i), a clean power law exponent $\chi = 1/2$ is found both numerically and analytically. In contrast, for the case (ii), analytical derivations are much more challenging, and the study of the system relies on numerical simulations. By fitting numerical data, one observes that the exponent χ depends on both the initial state and the strength of non-reciprocity; for instance $\chi = 0.58$ or $\chi = 0.515$ have been reported [27]. This non-trivial behaviour remains poorly understood and calls for the development of new theoretical frameworks.

In this article, we contribute to the studies on open and non-reciprocal quantum spin chains by proposing a theoretical approach based on the time-dependent generalized Gibbs ensemble (t-GGE) [30]. This framework applies to systems which are integrable in the absence of dissipation and are expected to thermalize to a generalized Gibbs ensemble (GGE) which maximizes the entropy while satisfying the extensive number of conservation laws of the Hamiltonian [31, 32]. When a weak dissipation is introduced, thereby breaking the conservation laws, the t-GGE approach postulates that the system should be described by a time-dependent GGE. This formalism has been used to describe various types of Lindbladian evolutions, such as lossy one-dimensional gases [33–37], reaction–diffusion dynamics in quantum gases [38, 39], digital quantum processors [40], trapped ions [41]. What makes t-GGE a well-established tool is that its predictions have been successfully validated through tensor-network simulations.

We show that the rapidity distribution is a crucial theoretical object for understanding the dissipative behaviour of a open non-reciprocal quantum spin chain. For the XX model considered in this work, the rapidity distribution coincides with the occupation numbers of fermionic quasiparticles that carry energy and magnetization, and that define a complete set of extensive conserved quantities. When the coherent part of the dynamics is governed by the XX Hamiltonian, we derive a closed set of differential equations whose number scales linearly with the system size, making them significantly cheaper to solve than tensor-network simulations. From the rapidity distribution, several physical observables can be directly computed, including the magnetization density and magnetization current, allowing us to formulate quantitative predictions and to provide a clear physical interpretation of the dynamics. Comparison with numerical simulations shows that this approach remains quantitatively accurate even in regimes where dissipation is not perturbative. In summary, we demonstrate that the physics of a class of open, non-reciprocal

quantum spin chains can be accessed by focusing solely on their rapidity distribution.

This work is organized as follows. In Sec. 2 we introduce the model of the open and non-reciprocal quantum spin chain that we will consider; we briefly review some known results and compare them with a simple theoretical analysis based on non-interacting fermions, which has several deficiencies. Our theoretical approach based on the t-GGE is presented in Sec. 3, where we derive a closed set of differential equations governing the time evolution of the rapidity distribution. By solving those equations, in Sec. 4 we theoretically study the temporal decay of the magnetization of the chain, whereas the onset of a non-reciprocal current is discussed in Sec. 5. Our conclusions are presented in Sec. 6. Six Appendices conclude the work. Throughout the article we set $\hbar = 1$.

2 Model and known results

2.1 The model

We consider a one-dimensional spin chain whose time evolution is governed by the XX Hamiltonian

$$H = -\frac{J}{2} \sum_j \left(S_{j+1}^+ S_j^- + S_j^+ S_{j+1}^- \right), \quad (1a)$$

where J is the exchange interaction, while $S_j^+ = (\sigma_j^x + i\sigma_j^y)/2$ and $S_j^- = (\sigma_j^x - i\sigma_j^y)/2$ denote the raising and lowering spin operators at the site j , respectively; σ^x and σ^y are Pauli matrices. We assume that this system is subject to two-site correlated dissipation as introduced in Ref. [27]: the time evolution of the system's density matrix ρ is modeled by the Lindblad master equation

$$\frac{d\rho}{dt} = -i[H, \rho] + \kappa \sum_j \left(L_j \rho L_j^\dagger - \frac{1}{2} \{ L_j^\dagger L_j, \rho \} \right), \quad (1b)$$

where the jump operators reads

$$L_j = S_j^- + e^{i\phi} S_{j+1}^-. \quad (1c)$$

Here, $\kappa > 0$ is the loss rate and $\phi \in (-\pi, \pi]$. The jump operators (1c) not only describe the decay of magnetization along the z -axis but also account for the presence of non-reciprocal interactions, leading to a transient magnetization current whenever $\phi \neq 0 \pmod{\pi}$ [21,27]. The strength of the non-reciprocity is controlled via both the loss rate κ and the phase ϕ ; for fixed κ , the non-reciprocity is maximal when $\phi = \pm\pi/2$ whereas the system is reciprocal when $\phi = 0, \pi$. We will consider translationally-invariant initial states of the form

$$|\Psi_0\rangle = \bigotimes_j \left(\cos \theta |\uparrow\rangle_j + \sin \theta |\downarrow\rangle_j \right), \quad \text{with } \theta \in [0, \frac{\pi}{2}). \quad (2)$$

Unless otherwise specified, we consider an infinite number of lattice sites and the boundary conditions do not matter. We denote the expectation value of an observable O as $\langle O \rangle(t) := \text{Tr}[O\rho(t)]$; in the following, the explicit time dependence (t) is often suppressed for brevity.

2.2 Known results on the algebraic decay of the magnetization

The spin model, described by the Eqs. (1), has been analyzed in Ref. [27] with tensor-network techniques. The authors computed the late-time decay of the local magnetization S_j^z via the proxy projector onto the $|\uparrow\rangle$ state,

$$n_j := S_j^+ S_j^-. \quad (3)$$

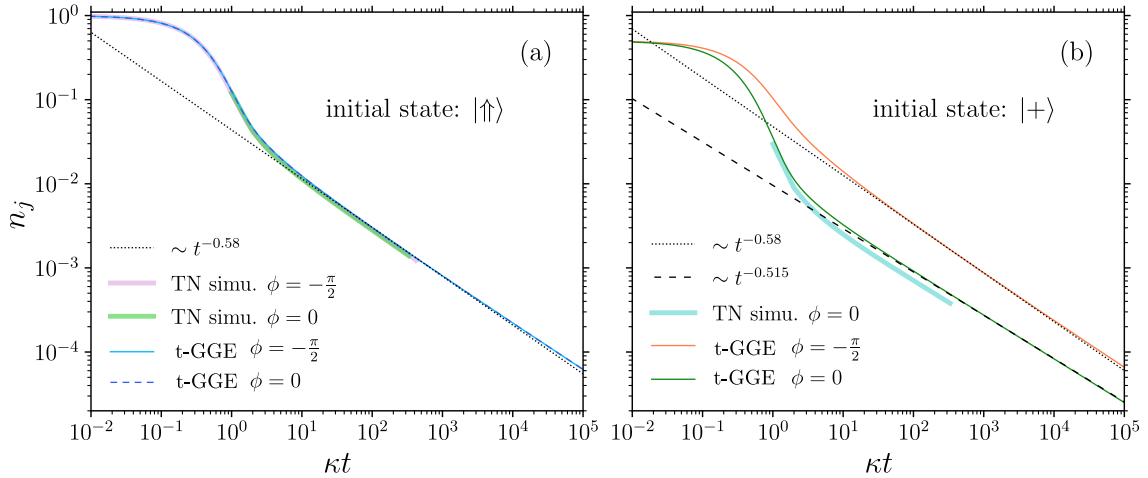


Figure 1: Time evolution of the local magnetization n_j defined in Eq. (3), for the two initial states $|\uparrow\rangle$ and $|+\rangle$, in both the reciprocal ($\phi = 0$) and maximally non-reciprocal ($\phi = -\pi/2$) cases. The wide lines are the results found in Ref. [27] via tensor-network (TN) simulations for open boundary conditions and $J/\kappa = 1$ (courtesy of the authors S.E. Begg and R. Hanai for sharing the data). For the purple curve on panel (a), the total number of lattice sites is $L = 500$ and the considered site $j = 450$; for both the green curve of panel (a) and the blue curve of panel (b), $L = 250$ and $j = L/2$. The thin lines are obtained via the t-GGE equation (21).

For open boundary conditions, and at late times, they observed an algebraic decay $\langle n_j \rangle \sim t^{-\chi}$ that depends on the initial state. By fitting the numerical data, they found $\chi = 0.58$ when initially all spins are up $|\uparrow\rangle = \bigotimes_j |\uparrow\rangle_j$, for both the reciprocal ($\phi = 0$) and maximally non-reciprocal ($\phi = -\pi/2$) cases. On the other hand, they fitted $\chi = 0.515$, for $\phi = 0$, when initially all spins are aligned along the x -direction $|+\rangle = \bigotimes_j \left(\frac{|\uparrow\rangle_j + |\downarrow\rangle_j}{\sqrt{2}} \right)$; their results are displayed as thick curves in Fig. 1.

In general, the algebraic decays of observables are a consequence of the closure of the Lindbladian gap and the presence of slow modes in the thermodynamic limit: the system is then called critical. This phenomenon is widely observed in the literature [19, 29, 42–45]. By empirical observation, the power law exponents are typically rational numbers of the form $-p/q$ where both p and q are small (for instance -1 or $-1/2$). Therefore, these power law exponents -0.58 and -0.515 are rather unexpected.

2.3 Free fermions

As a first step towards analyzing the spin model introduced above, we follow Refs. [27, 29] and consider an exactly solvable free fermionic model whose Hamiltonian and jump operators are

$$H = -\frac{J}{2} \sum_j \left(c_{j+1}^\dagger c_j + c_j^\dagger c_{j+1} \right), \quad L_j = c_j + e^{i\phi} c_{j+1}. \quad (4)$$

Here, c_j^\dagger and c_j denote the creation and annihilation operators of a fermion at site j . We consider this model because, as will be shown in the upcoming section, it is closely related to the one described by Eqs. (1), even though not equivalent to it. To investigate the

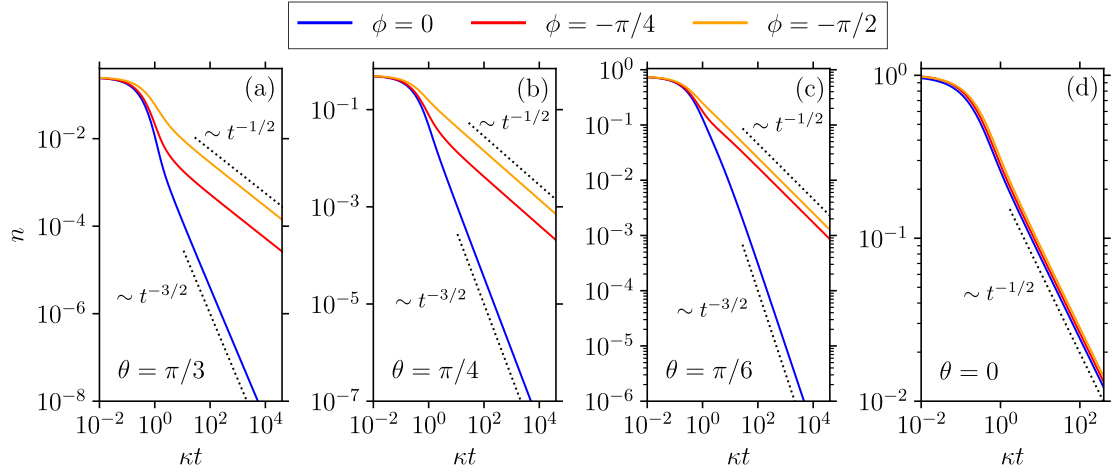


Figure 2: Time evolution of the local fermion density n for the model (4) for several non-reciprocity angles $\phi = 0, -\pi/4, -\pi/2$. Different panels correspond to different initial states, parametrized by θ according to the expression in Eq. (8): panel (a), $\theta = \pi/3$; panel (b), $\theta = \pi/4$ corresponding to $|\Psi_0\rangle = |+\rangle$; panel (c), $\theta = \pi/6$; panel (d), $\theta = 0$ corresponding to $|\Psi_0\rangle = |\uparrow\rangle$. The colored continuous curves are obtained by numerically evaluating the integral (11). The dotted curves are guides to the eye for the late-time power-law scaling. In panel (d), all the curves overlap perfectly; the curves for $\phi = 0, -\pi/4$ have been slightly shifted to improve visibility.

model (4), we introduce the Fourier modes

$$\forall k \in [0, 2\pi), c^\dagger(k) = \frac{1}{\sqrt{2\pi}} \sum_{j=-\infty}^{+\infty} e^{ikj} c_j^\dagger, \quad c_j^\dagger = \frac{1}{\sqrt{2\pi}} \int_0^{2\pi} e^{-ikj} c^\dagger(k) dk, \quad (5)$$

and the rapidity distribution $\varrho(k)$ defined via

$$\langle c^\dagger(k) c(q) \rangle = \delta(k - q) \varrho(k). \quad (6)$$

Note that $\langle c^\dagger(k) c(q) \rangle = 0$ when $k \neq q$ is a direct consequence of the translational invariance of the system (see Appendix A for a proof). The initial state (2) can be written in the fermionic basis using the Jordan-Wigner transform

$$c_j = (-1)^{N_{(-\infty, j-1)}} S_j^-, \quad c_j^\dagger = (-1)^{N_{(-\infty, j-1)}} S_j^+, \quad \text{with} \quad N_{(-\infty, j)} = \sum_{l=-\infty}^j n_l. \quad (7)$$

We then have

$$|\Psi_0\rangle = \dots \left(\cos \theta c_1^\dagger + \sin \theta \right) \left(\cos \theta c_2^\dagger + \sin \theta \right) \left(\cos \theta c_3^\dagger + \sin \theta \right) \dots |\text{vac}\rangle, \quad (8)$$

where $|\text{vac}\rangle = \bigotimes_j |\downarrow\rangle_j$ is the vacuum state. The rapidity distribution of $|\Psi_0\rangle$ is

$$\varrho_0(k) = \begin{cases} \frac{2 \cos^4(\theta) (1 + \cos(k))}{1 + 2 \cos(k) \cos(2\theta) + \cos^2(2\theta)}, & \text{if } \theta \in (0, \frac{\pi}{2}), \\ 1, & \text{if } \theta = 0. \end{cases} \quad (9)$$

(see Appendix B for details). Using the free fermionic nature of the model, we can show that [27, 29]

$$\frac{d}{dt}\varrho(k) = -2\kappa(1 + \cos(\phi + k))\varrho(k). \quad (10)$$

Hence, the time-dependent translationally-invariant density of fermions is

$$n(t) := \langle n_j \rangle(t) = \langle c_j^\dagger c_j \rangle(t) = \int_0^{2\pi} \frac{dk}{2\pi} \varrho(k, t) = \int_0^{2\pi} \frac{dk}{2\pi} \varrho_0(k) e^{-2\kappa(1+\cos(\phi+k))t}. \quad (11)$$

From the Eqs. (9) and (11), we can easily compute numerically the time evolution of n , as shown in Fig. 2. At late time, we observe power-law behaviors $n \sim t^{-\chi}$ with

$$\chi = \begin{cases} 3/2, & \text{if } \phi = 0 \text{ and } \theta \in (0, \frac{\pi}{2}), \\ 1/2, & \text{otherwise.} \end{cases} \quad (12)$$

This can be shown analytically; see Appendix C for a proof. Thus, already at the level of free fermions we find that different power-law exponents χ emerge, depending both on the strength of the non-reciprocity and on the initial state. In particular, the configurations $(\phi = 0, \theta = 0)$ and $(\phi = -\pi/2, \theta = 0)$ yield the same value of χ , whereas the case $(\phi = 0, \theta = \pi/4)$ does not, mirroring the behavior reported previously for the analogous spin system in Ref. [27]. Once more, we observe that in this situation where an analytical calculation could be performed, the value of χ takes a simple rational form.

3 Time-dependent generalized Gibbs ensemble (t-GGE)

In this section, we present our theoretical framework for the study of the spin model described by Eqs. (1). Crucially, we assume that the system is weakly dissipative *i.e.* $\kappa \ll J$; as a consequence, the coherent unitary dynamics occurs on a much shorter time scale than that of the loss processes. In this context, it is customary to assume that the system relaxes locally to a time-dependent generalized Gibbs ensemble (t-GGE) [30, 33, 34, 36, 37, 39, 40].

3.1 t-GEE for the spin model in Eqs. (1) on an infinite lattice

First, we map the spin operators S_j^+, S_j^- to the fermionic operators c_j^\dagger, c_j via the Jordan-Wigner transform (7). Under this transformation, the Hamiltonian and the jump operators can then be rewritten as

$$H = -\frac{J}{2} \sum_{j=-\infty}^{+\infty} \left(c_j^\dagger c_{j+1} + c_{j+1}^\dagger c_j \right), \quad L_j = (-1)^{N_{(-\infty, j-1)}} \left(c_j + e^{i\phi} (-1)^{n_j} c_{j+1} \right). \quad (13)$$

We note that our spin model is different from the free fermions (4) because of the strings $(-1)^{N_{(-\infty, j-1)}}$ and $(-1)^{n_j}$ appearing in L_j . This is the essence of the difference between the two approaches; the importance of Jordan-Wigner strings in open quantum system dynamics has been recently highlighted in Ref. [46].

The Hamiltonian is diagonal in Fourier space:

$$H = \int_0^{2\pi} \epsilon_k c^\dagger(k) c(k) dk, \quad \text{with } \epsilon_k = -J \cos k. \quad (14)$$

Thus, we can identify the mutually commuting and extensive operators which also commute with H , also known as the extensive charges. Denoting them as $\{Q_m\}$, we have

$[Q_m, H] = [Q_m, Q_n] = 0$. We recall that, by definition, if Q_m is extensive then it can be written as $Q_m = \sum_j q_{j,m}$ where $q_{j,m}$ is its density operator and acts on a finite number of sites around j (*i.e.* has a finite support). From the expression of H in Eq. (14), we see that the charges can be expressed as

$$Q_{2p} = \int_0^{2\pi} \sin(pk) c^\dagger(k) c(k) dk, \quad (15a)$$

$$Q_{2p+1} = \int_0^{2\pi} \cos(pk) c^\dagger(k) c(k) dk; \quad \forall p \in \{0, 1, 2, \dots\}. \quad (15b)$$

In the absence of losses, *i.e.* $\kappa = 0$, the system would relax to a generalized Gibbs ensemble (GGE) characterized by $\{Q_m\}_{m>0}$. However, in the case of weak adiabatic losses, the integrability is weakly broken, meaning that the GGE is not exactly stationary. Therefore, we assume that the system's density matrix is locally indistinguishable from

$$\rho_{\text{GGE}}(t) = \frac{e^{-\sum_m \beta_m(t) Q_m}}{\text{Tr}[e^{-\sum_m \beta_m(t) Q_m}]}, \quad (16)$$

where the Lagrange multipliers $\beta_m(t)$ are slowly varying in time. The state (16) is called a t-GGE and can also be expressed as

$$\rho_{\text{GGE}}(t) = \frac{1}{\mathcal{Z}(t)} e^{-\int \lambda_k(t) c^\dagger(k) c(k) dk}, \quad (17)$$

with $\lambda_k(t) = \sum_p \beta_{2p+1}(t) \cos(pk) + \beta_{2p}(t) \sin(pk)$ and $\mathcal{Z}(t)$ is the appropriate normalization constant. Remarkably, the state (17) is a Gaussian fermionic state; this property will be used in order to apply the Wick theorem.

3.2 Equation of motion for the rapidity distribution

We aim to derive a closed set of dynamical equations for the rapidity distribution $\varrho(k)$ defined in Eq. (6). For this, we will follow similar steps as in Refs. [33, 36]. From the Lindblad master equation (1b), we obtain

$$\frac{d}{dt} \langle c^\dagger(k) c(k) \rangle = -\kappa \sum_{j=-\infty}^{\infty} \left(\text{Re} \left[\langle L_j^\dagger L_j c^\dagger(k) c(k) \rangle \right] - \langle L_j^\dagger c^\dagger(k) c(k) L_j \rangle \right). \quad (18)$$

Using the Eqs. (6) and (18), and the translational invariance, we find

$$-\frac{1}{2\pi\kappa} \frac{d\varrho(k)}{dt} = \text{Re} \left[\langle L_j^\dagger L_j c^\dagger(k) c(k) \rangle \right] - \langle L_j^\dagger c^\dagger(k) c(k) L_j \rangle. \quad (19)$$

By assuming that the density matrix of the system is locally indistinguishable from the t-GGE (17), we can show

$$\begin{aligned} -\frac{1}{2\kappa} \frac{d\varrho(k)}{dt} &= \varrho(k) (1 - \varrho(k)) (1 + \cos(k + \phi)) + 2 \left(\int_0^{2\pi} \frac{dq}{2\pi} \varrho(q) \frac{\cos\left(\frac{q+\phi}{2}\right)}{\sin\left(\frac{k-q}{2}\right)} \right)^2 \\ &+ \int_0^{2\pi} \frac{dq}{2\pi} \varrho(q) (1 + \cos(q + \phi)) \int_0^{2\pi} \frac{dp}{2\pi} \frac{\varrho(k) - \varrho(p)}{\sin^2\left(\frac{k-p}{2}\right)}. \end{aligned} \quad (20)$$

The notation \int denotes the Cauchy principal value of the integral. Eq. (20) is the main result of this article; its complete derivation is provided in Appendix D.

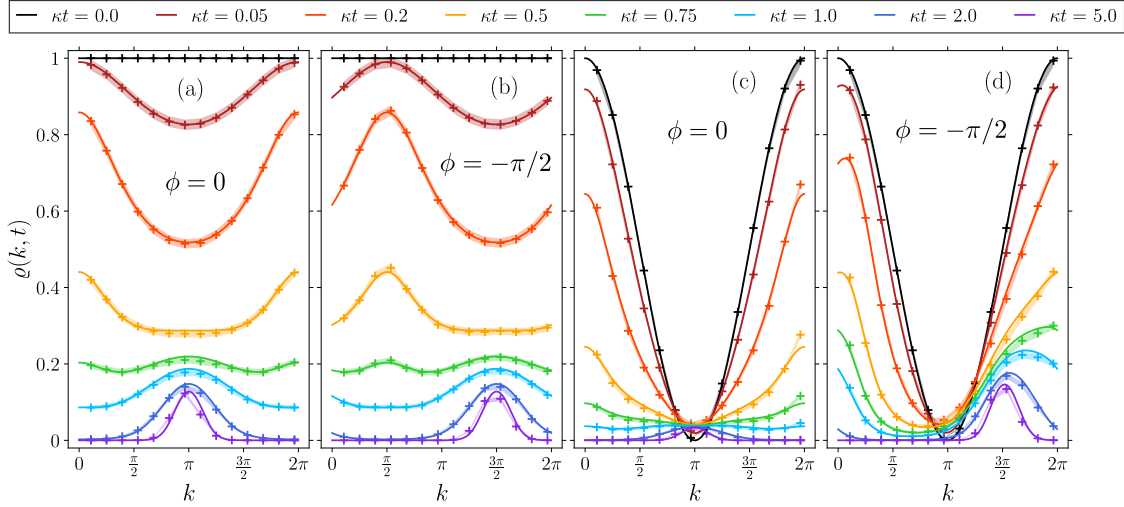


Figure 3: Time evolution of the rapidity distribution $\varrho(k, t)$. Different panels refer to different initial states and angles ϕ : (a) $|\uparrow\rangle$ and $\phi = 0$; (b) $|\uparrow\rangle$ and $\phi = -\pi/2$; (c) $|+\rangle$ and $\phi = 0$; (d) $|+\rangle$ and $\phi = -\pi/2$. For all panels, the continuous curves are obtained by solving numerically the Eq. (21). On the other hand, the crosses correspond to a finite lattice of $L = 14$ sites where computations are performed via a quantum trajectory stochastic algorithm, averaging over 5000 trajectories, with the parameters $J = 1$ and $\kappa = 0.02$, and periodic boundary conditions.

In order to solve numerically the latter equation, we use the following alternative form, involving circular Hilbert transforms,

$$\begin{aligned} -\frac{1}{2\kappa} \frac{d\varrho(k)}{dt} = & (\varrho(k) + \varrho_c(k)) (1 - \varrho(k)) + n \left(n + 2\mathcal{H}[\varrho]'(k) + \mathcal{H}[\varrho_s](k) + \int_0^{2\pi} \frac{dq}{2\pi} \varrho_c(q) \right) \\ & + \mathcal{H}[\varrho](k) \times \left(\mathcal{H}[\varrho](k) + \mathcal{H}[\varrho_c](k) - \int_0^{2\pi} \frac{dp}{2\pi} \varrho_s(p) \right) + 2\mathcal{H}[\varrho]'(k) \int_0^{2\pi} \frac{dq}{2\pi} \varrho_c(q). \end{aligned} \quad (21)$$

Here,

$$n = \int_0^{2\pi} \frac{dk}{2\pi} \varrho(k) \quad (22)$$

is the fermion density, which is related to the magnetization density via Eq. (3); we have used the short-hand notations $\varrho_c(k) = \varrho(k) \cos(k + \phi)$, $\varrho_s(k) = \varrho(k) \sin(k + \phi)$. In addition, we recall the definition of the circular Hilbert transform and the expression of its derivative [47, 48]:

$$\mathcal{H}[f](k) = \int_0^{2\pi} \frac{dp}{2\pi} \cot\left(\frac{k-p}{2}\right) f(p), \quad \mathcal{H}[f]'(k) = \frac{1}{2} \int_0^{2\pi} \frac{dp}{2\pi} \frac{f(k) - f(p)}{\sin^2\left(\frac{k-p}{2}\right)}. \quad (23)$$

The procedure used to solve numerically Eq. (21) is detailed in Appendix E.

3.3 The time-evolving rapidity distribution

In Fig. 3, we show the distribution $\varrho(k)$ at various times, for two different initial states, $|\uparrow\rangle$ and $|+\rangle$ corresponding to $\theta = 0, \pi/4$ respectively, in both the reciprocal ($\phi = 0$) and maximally non-reciprocal ($\phi = -\pi/2$) cases. On this figure, we compare the results given

by solving numerically Eq. (21) and the exact simulation of the model via a stochastic quantum trajectory algorithm for a finite system of $L = 14$ sites. The calculation is performed with the open-source python-framework QuTiP [49, 50]. Details on how to take care of the finite size of the system and of its boundary conditions can be found in Appendix F. We obtain a good agreement between the two methods.

In all simulations presented in Fig. 3, $\varrho(k)$ tends to develop a peak around the wavevector $k^* = \pi - \phi$ at late time; this is compatible with the presence of long-lived modes around k^* as predicted in Ref. [27]. The latter can be understood by noticing that, at late time, the system is almost empty (almost all the spins are down in the spin language), meaning that $n_j \approx 0, \forall j$; thus, we can approximate the string operators as $(-1)^{N_{(-\infty, j-1)}} \approx 1$ and $(-1)^{n_j} \approx 1$. The jump operators (13) are then approximately equal to the free fermionic ones *i.e.* $L_j \approx c_j + e^{i\phi} c_{j+1}$; therefore the rapidity distribution is approximately governed by the Eq. (10) which features slow-decaying modes around $k = k^*$, as it is obvious from the dynamical equation (10).

On the other hand, following this line of reasoning, in some situations the short-time dynamics can be well approximated by a free-fermion one. Indeed, when the initial state is $|\Psi_0\rangle = |\uparrow\rangle$, we see that $\varrho(k)$ first develops a peak around $\tilde{k} = -\phi$ before developing one around k^* . At short time, we can appropriate $(-1)^{n_j} \approx -1$ and the string operator $(-1)^{N_{(-\infty, j-1)}}$ reduces to an irrelevant scalar number. As a consequence, the jump operators (13) become $L_j \approx c_j - e^{i\phi} c_{j+1} = c_j + e^{i(\phi+\pi)} c_{j+1}$, and the system behaves like the free fermionic model (4) with a non-reciprocity angle shifted by π *i.e.* $\phi \rightarrow \phi + \pi$. Thus, in the short-time regime, we have $\frac{d}{dt}\varrho(k) \approx -2\kappa(1 - \cos(k + \phi))\varrho(k)$, and slow-decaying modes accumulate around $k = \tilde{k}$.

We also note that, if the initial state is $|\uparrow\rangle$, then the initial rapidity distribution $\varrho_0(k) = 1$ is uniform; thus varying the non-reciprocity angle ϕ amounts simply to a global translation in momentum space (see Figs. 3(a) and 3(b)). On the contrary, if the initial state is $|+\rangle$, which corresponds to the initial rapidity distribution $\varrho_0(k) = (1 + \cos(k)) / 2$, then varying ϕ has a non-trivial effect on $\varrho(k, t)$ (see Figs. 3(c) and 3(d)).

4 Time decay of the magnetization

4.1 Comparison between the t-GGE results and tensor-network simulations

We focus on the dynamics of the local magnetization n , defined in Eq. (22); we could not find a closed expression for the dynamics of $n(t)$ starting from those for the rapidity distribution in Eq. (20), hence we obtain it by numerical integration of the numerical solution for $\rho(k)$ discussed in Sec. 3.3. We check that this method is consistent with exact simulations of a small system of $L = 14$ sites using quantum trajectories, for times up to $\kappa t = 5$, as shown in Fig. 4. We compute n with quantum trajectories for both $\kappa/J = 0.02$ and $\kappa/J = 1$. As anticipated, the t-GGE equations (21) give accurate results in the weakly dissipative regime $\kappa \ll J$. Moreover, it also provides surprisingly good predictions in the case $\kappa/J = 1$ when the initial state is $|\uparrow\rangle$ (see Figs. 4(a) and (b)). This is not the case for $\rho(k)$: however, errors are averaged out by the integral in Eq. (22).

Let us now focus on the tensor-network simulations of n presented in Ref. [27], which have been performed for significantly large systems composed of $L = 250$ or 500 sites, whose results have been already discussed and presented in Fig. 1. We now compare those results with those obtained with our t-GGE method (21), which are also displayed in Fig. 1 for the four cases obtained by considering both $\phi = 0, -\pi/2$ and initializing the

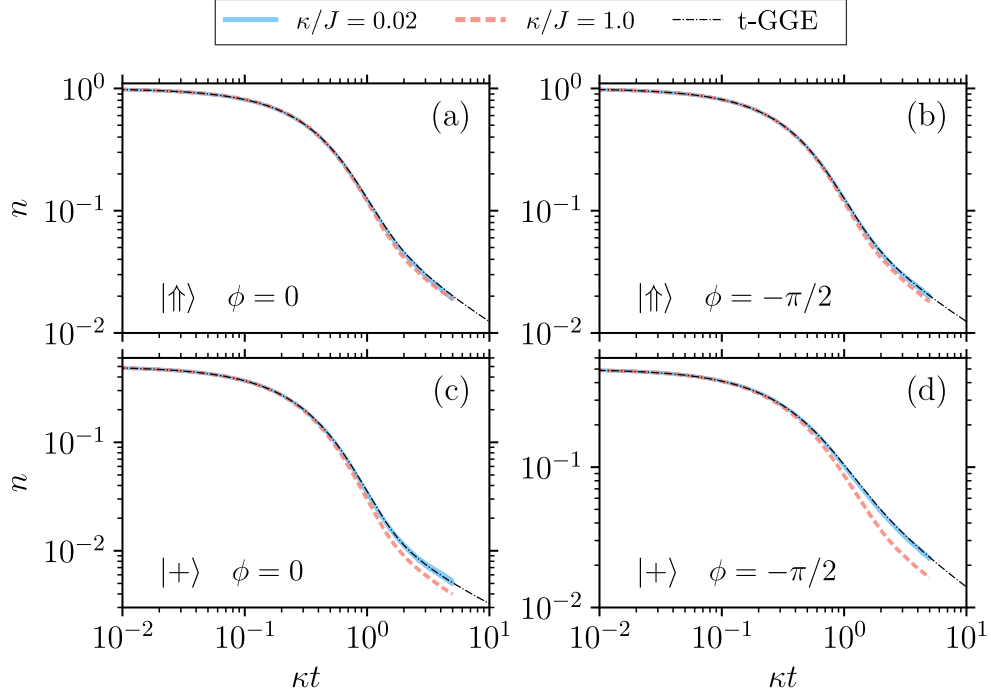


Figure 4: Short time evolution of the local magnetization n , for the two initial states $|\uparrow\rangle$ and $|+\rangle$, in both the reciprocal ($\phi = 0$) and maximally non-reciprocal ($\phi = -\pi/2$) cases. The colored curves are obtained via a stochastic quantum trajectory algorithm with 5000 trajectories for $L = 14$ lattice sites, with periodic boundary conditions. The parameters are $J = 1$, $\kappa = 0.02$ (continuous blue) or $\kappa = 1$ (dashed red). The dash-dotted black curves are obtained by solving Eq. (21) and integrating the resulting rapidity distribution numerically.

system in both states $|\Psi_0\rangle = |\uparrow\rangle, |+\rangle$. When the comparison is possible, the agreement is surprisingly good, especially if we consider that the tensor-network simulations are performed in a regime, $\kappa = J$, where our perturbative approach is not expected to work. More precisely, we see that our results and the simulations of Ref. [27] superimpose when $|\Psi_0\rangle = |\uparrow\rangle$, see Fig. 1 (a), while a vertical shift is present when $|\Psi_0\rangle = |+\rangle$, see Fig. 1 (b). We also mention that, from the discussion of Sec. 3.2, it is clear that, for $|\Psi_0\rangle = |\uparrow\rangle$, the dynamics of n is completely insensitive to the value of ϕ , since varying ϕ results only in a global shift of the distribution $\varrho(k)$ in momentum space.

4.2 Late-time decay

We now focus specifically on the behavior of the magnetization at late times. Fig. 1 shows that in all situations, for times $50 \gtrsim \kappa t \gtrsim 10^4$, the t-GGE approach yields power-law decays that are compatible with those of the tensor-network data. Specifically, we observe $n \sim t^{-\chi}$ where $\chi = 0.58$ for $|\Psi_0\rangle = |\uparrow\rangle$ and $\phi = 0, -\pi/2$, while $\chi = 0.515$ for $|\Psi_0\rangle = |+\rangle$ and $\phi = 0$. We also report that $\chi = 0.58$ for $|\Psi_0\rangle = |+\rangle$ and $\phi = -\pi/2$, a situation that is not considered in Ref. [27].

The t-GGE methods allows us to access time scales much larger than those reachable via tensor-network simulations, such as those employed in Ref. [27], which do not exceed $\kappa t \sim 10^3$. By pushing our numerics to times as long as $\kappa t \sim 10^5$ we can inspect whether the identified scalings $t^{-\chi}$ persist at larger times. When the initial state is $|\uparrow\rangle$, we observe

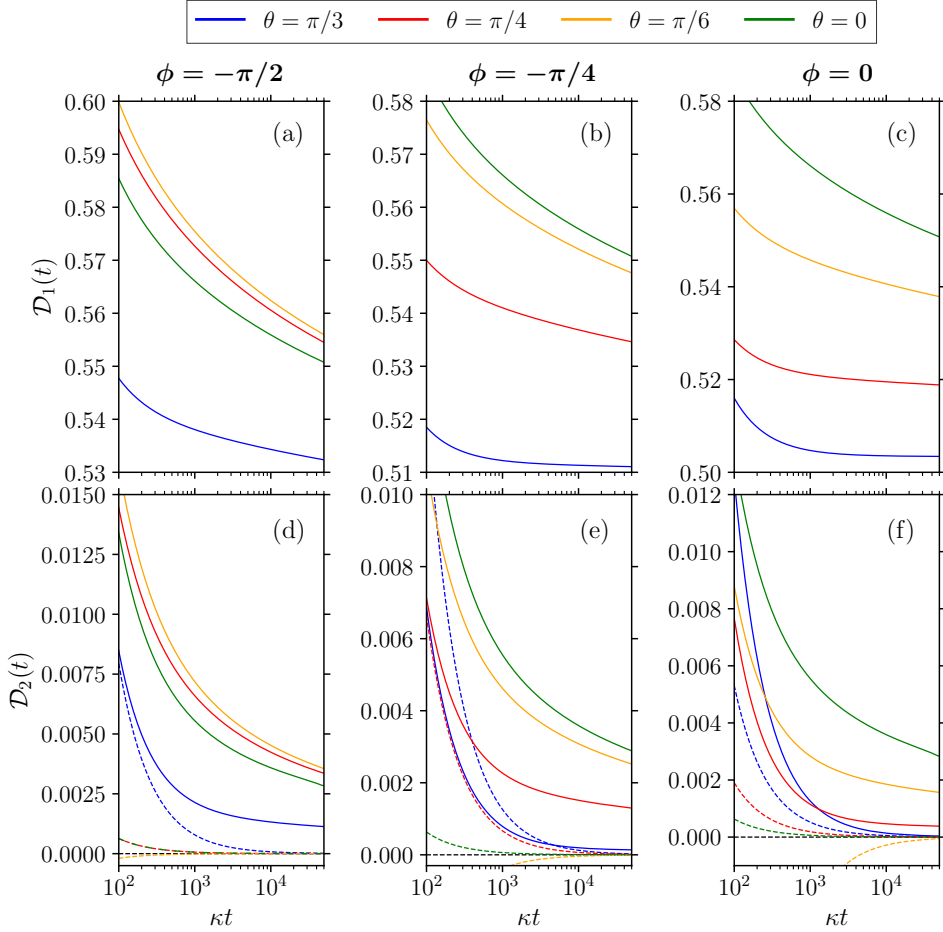


Figure 5: First and second logarithmic derivatives of n , for various initial states parameterized by θ and various strength of non-reciprocity ϕ . The continuous curves are obtained via the t-GGE approach in Eq. (21) describing the dynamics of the spin model. The dashed curves in panels (d-f) are obtained via the dynamical Eqs. (10) describing the time-evolution of the free fermionic model (4).

a small but significant deviation from a pure power law decay in the time window $10^4 \gtrsim \kappa t \gtrsim 10^5$, as it is visible in Fig. 1(a). To investigate this behavior, we analyze the first and second logarithmic derivatives of $n(\kappa t)$ with respect to $\log(\kappa t)$, defined respectively as

$$\mathcal{D}_1(t) := -\frac{d \log(n)}{d \log(\kappa t)} \quad \text{and} \quad \mathcal{D}_2(t) := \frac{d^2 \log(n)}{(d \log(\kappa t))^2}. \quad (24)$$

For a pure algebraic decay $n \sim (\kappa t)^{-\chi}$, the first logarithmic derivative is time-independent and equal to the critical exponent χ , while the second logarithmic derivative vanishes: $\mathcal{D}_1(t) = \chi$ and $\mathcal{D}_2(t) = 0$.

The numerical results are presented in Fig. 5 for several values of the non-reciprocity parameter $\phi = -\pi/2, -\pi/4, 0$ and for different initial states parametrized by the angles $\theta = \pi/3, \pi/4, \pi/6, 0$. For most values of the angles θ and ϕ , we observe that $\mathcal{D}_1(t)$ continues to decay without approaching a stationary value, and that $\mathcal{D}_2(t)$ remains finite over the entire time window accessible with the t-GGE method. We thus conclude that $n(t)$ is not converging towards a purely algebraic decay behavior within the probed time scales; the only exception to this seems to be the case $\theta = \pi/3$ and $\phi = 0$. In contrast,

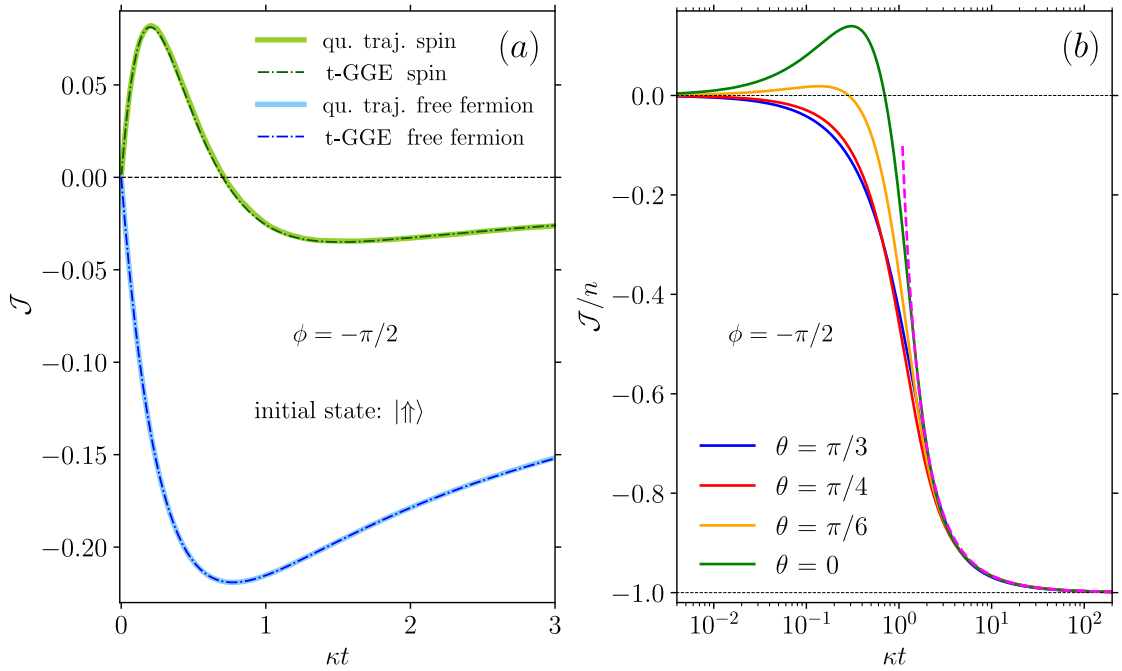


Figure 6: (a) Time evolution of the magnetization current for the spin system described by Eqs. (1) (in green), and for the free fermionic system described by Eqs. (4) (in blue). The initial state is $|\uparrow\uparrow\rangle$ and the non-reciprocity is maximal, i.e. $\phi = -\pi/2$. The dash-dotted curves are obtained by solving numerically the t-GGE equations (21) and the dynamical equations (10), respectively, for the integral expression of the current $J = J \int dk \sin(k) \varrho(k)/2\pi$. The continuous curves are obtained via stochastic quantum trajectories averaging over 5000 trajectories, with periodic boundary conditions and $\kappa/J = 0.01$. For the free fermions, we use $L = 10$ lattice sites; for the spin system, we use $L = 14$ lattice sites. (b) Time evolution of the ratio J/n for $\phi = -\pi/2$ and for various initial states parametrized by the angle θ , in the case of the spin system. The continuous curves are obtained via the t-GGE equations (21). The dashed magenta curve is $f(\kappa t) = \sin(\phi) (1 - \sigma(\kappa t)^2/2)$ where $\sigma(\kappa t)$ is obtained by fitting the rapidity distribution at time t with the gaussian (26), in the case $\theta = 0$. For both panels (a) and (b), $J = 1$.

for the same time interval, we see that the free fermionic system displays a power-law behavior since $\mathcal{D}_2(t)$ reaches zero (see dashed lines in Figs. 5 (d) (e) (f)).

Based on these numerical observations, it remains unclear whether (i) the magnetization in the spin system eventually crosses over to a true algebraic decay at extremely late times, or (ii) a deviation from power-law behavior persists asymptotically, so that the spin system's late-time relaxation is different in essence for the one of free fermions. In a previous work, we have highlighted the fact that in some lattice models the late-time decay could display a logarithmic correction that could be extremely difficult to fit [45]; it is still to be understood whether this is also what happens here.

5 Hamiltonian magnetization current

In this section, we discuss several properties of the Hamiltonian magnetization current density, defined as

$$\mathcal{J} := \left\langle \frac{iJ}{2} \left(S_{j+1}^+ S_j^- - S_j^+ S_{j+1}^- \right) \right\rangle = \left\langle \frac{iJ}{2} \left(c_{j+1}^\dagger c_j - c_j^\dagger c_{j+1} \right) \right\rangle = J \int_0^{2\pi} \frac{dk}{2\pi} \sin(k) \varrho(k). \quad (25)$$

We recall that in our problem the latter is invariant by translation in real space, hence the absence of a dependence on j in the final expression. Note that this is not the operator that satisfies the continuity equation for the magnetization under the dissipative dynamics, but only under the Hamiltonian one [21, 29].

We first remark that, depending on the strength of the non-reciprocity $\phi \neq 0$ and the initial state, a sign reversal of the current can occur dynamically for the spin system, while this phenomenon is totally absent for the analogous free fermionic system. This behavior occurs for instance when $|\Psi_0\rangle = |\uparrow\rangle$ and $\phi = -\pi/2$ as shown in Fig. 6(a): we indeed observe a reversal of the current sign for the spin system, while the current remains negative at all times for the free fermions. As shown in Fig. 3(b), the rapidity distribution $\varrho(k)$ develops a peak at momenta between 0 and π at short times, which implies $\mathcal{J} > 0$. At later times, however, a second peak necessarily emerges at momenta between π and 2π , resulting in $\mathcal{J} < 0$. The different behaviour at high and low fillings can be understood with the simple arguments proposed in Sec. 3.3 and mapping the dynamics to two different models in the two cases.

Another straightforward consequence of the fact that the slow-decaying modes are located around $k^* = \pi - \phi$ is that the ratio \mathcal{J}/n becomes constant and equal to $J \sin(\phi)$ in the limit $t \rightarrow \infty$, as shown in Fig. 6(b). Indeed, at late times the distribution $\varrho(k)$ is sharply peaked around k^* , which allows us to perform a saddle-point approximation: $\mathcal{J} = J \int_0^{2\pi} dk \varrho(k) \sin(k) / 2\pi \approx J \sin(k^*) \int_0^{2\pi} dk \varrho(k) / 2\pi = J \sin(k^*) n$. Similarly, the ratio between density of energy $\varepsilon := -J \int_0^{2\pi} dk \cos(k) \varrho(k) / 2\pi$ and n tends to $J \cos(\phi)$ when $t \rightarrow \infty$; the ratio \mathcal{J}/ε tends to $\tan(\phi)$.

We note that the way \mathcal{J}/n approaches its stationary value gives information about the standard deviation of the rapidity distribution. For instance, in the case $|\Psi_0\rangle = |\uparrow\rangle$, at late time the rapidity distribution is well-approximated by a gaussian of the form

$$\varrho(k, t) = \mathcal{A}(\kappa t) \exp(-(k - k^*)^2 / 2\sigma(\kappa t)^2), \quad (26)$$

where $\mathcal{A}(\kappa t)$ and $\sigma(\kappa t)$ are time-dependent functions. Thus, by Taylor expanding $\sin(k)$ up to the $O(k^2)$ order, we find after a few algebraic manipulations that

$$\mathcal{J}/n \approx \sin(\phi) (1 - \sigma(\kappa t)^2 / 2). \quad (27)$$

The latter identity is checked numerically via the rate equation (21), see Fig. 6(b).

6 Conclusion and perspectives

We have presented a study based on the time-dependent generalized Gibbs ensemble of the dissipative dynamics of an open and non-reciprocal quantum spin chain. This problem, that has already been the object of several previous publications, is characterized by various peculiar properties, such as the fact that a current is dynamically established only due to the dissipative dynamics [21]. Extensive tensor-network simulations have

shown some peculiar properties of the power law that describes the temporal decay of the magnetization of the chain [27].

We believe that the main interest of this approach is to provide a simple theoretical framework for dealing with a Markovian open quantum spin chain, whose coherent dynamics is governed by the XX model; our framework produces controlled and accurate predictions in the limit of small dissipation, while producing data with an almost quantitative agreement also for larger dissipation strengths. The Eqs. (20) and (21) constitute the main result of our work, and, although they do not seem to be amenable to a simple analytical solution, they can be easily solved numerically. The plot in Fig. 3 shows the main physical message of our work, namely the dynamics of the rapidity distribution under this non-reciprocal dynamics. Non-reciprocity is responsible for the development of a rapidity distribution that is not symmetric under the exchange $k \rightarrow -k$, and that develops a magnetization current. In Fig. 6 we have shown that the Hamiltonian current of the model can display an intriguing switch of direction during the time evolution.

Another problem that we addressed is that of the power-law decay of the magnetization of the spin chain, which was shown in Ref. [27] to be characterised by rather unusual power-law exponents. Our study can access longer time scales and suggests that this exponent may depend on time; it is possible, although we have not been able to show it, that a logarithmic correction to the power-law appears, as we were able to show in another model, discussed in Ref. [45]. It is however important to stress that unusual power-law exponents have been reported also in numerical studies of other models, such as in Ref. [42]: the problem deserves further attention.

For a more general setting such as a Lindbladian system with an interacting integrable Hamiltonian, the associated t-GGE ensemble is generally non-Gaussian, which makes the problem challenging to treat analytically. Nevertheless, the t-GGE approach has successfully been applied to a Lieb-Liniger gas with finite interaction strength and local K -body losses (with $K = 1, 2, 3$) [33]. In principle, a similar framework could be used to study a non-reciprocal open quantum system with coherent dynamics described by the XXZ model, although a simple set of closed equations such as those in Eq. (20) are not expected to exist.

The main theoretical perspective of our work is to give an analytical solution of the t-GGE Eqs. (20) or (21). If this does not appear to be possible during the entire time dynamics, it may be possible to deduce analytically the late-time limit of the equations, as it was done in Refs. [34, 45], thereby clarifying completely the questions presented by the numerical solution of this problem.

More generally, this work suggests the importance of considering with appropriate theoretical tools that go beyond simple mean-field treatments the dynamics of integrable models, such as the XX quantum spin chain, when integrability is weakly broken, in this case by non-reciprocal losses. This poses the intriguing question of how to study the action of non-reciprocal losses in the case of a quantum spin chain that does not support the Hamiltonian magnetization current as a conservation law. Such models exist, and many non-integrable models have this property. Whether external reservoirs could induce a current flow also in those situations is an intriguing question that deserves to be studied.

Acknowledgements

We thank G. Aupetit-Diallo, S. E. Begg, M. Brunelli, J. Dubail, R. Hanai, L. Lumia, and M. Schirò for enlightening discussions. We are extremely grateful to S. E. Begg and R. Hanai for sharing their numerical data. AM, AN and LM thank the University of Tokyo

for warm hospitality.

Funding information This work was carried out in the framework of the joint Ph.D. program between the CNRS and the University of Tokyo. This work is supported by the ANR project LOQUEST ANR-23-CE47-0006-02 and by the PEPR Dyn-1D ANR-23-PETQ-0001. This work is part of HQI (www.hqi.fr) initiative and is supported by France 2030 under the French National Research Agency grant number ANR-22-PNCQ-0002. H.K. was supported by JSPS KAKENHI Grants No. JP23K25783, No. JP23K25790, and MEXT KAKENHI Grant-in-Aid for Transformative Research Areas A “Extreme Universe” (KAKENHI Grant No. JP21H05191).

A Proof that $\langle c^\dagger(k)c(q) \rangle = 0$ for $k \neq q$

In this appendix, we show that $\langle c^\dagger(k)c(q) \rangle = 0$, for $k \neq q$, is a direct consequence of the translational invariance of the system. By going back to real space, we find

$$2\pi\langle c^\dagger(k)c(q) \rangle = \sum_{j=-\infty}^{\infty} \sum_{l=-\infty}^{\infty} e^{ikj} e^{-iql} \langle c_j^\dagger c_l \rangle = \sum_{j=-\infty}^{\infty} \sum_{\eta=-\infty}^{\infty} e^{i(k-q)j} e^{-iq\eta} \langle c_j^\dagger c_{j+\eta} \rangle \quad (28)$$

From the translational invariance, we obtain that, for all $\eta \in \mathbb{Z}$, $\langle c_j^\dagger c_{j+\eta} \rangle =: f(\eta)$ is independent of the lattice site. Thus,

$$2\pi\langle c^\dagger(k)c(q) \rangle = \underbrace{\left[\sum_{j=-\infty}^{\infty} e^{i(k-q)j} \right]}_{=0 \text{ if } k \neq q} \left[\sum_{\eta=-\infty}^{\infty} f(\eta) e^{iq\eta} \right] \quad (29)$$

Therefore, if $k \neq q$ then $\langle c^\dagger(k)c(q) \rangle = 0$. This justifies the form of the Eq. (6).

B Derivation of Eq. (9)

In this appendix, we show how to obtain the rapidity distribution associated with the initial state (2), written as (8) in the fermionic language. First we note that

$$\underbrace{\delta(k-q)}_{\frac{1}{2\pi} \sum_j e^{i(k-q)j}} \varrho_0(k) = \langle \Psi_0 | c^\dagger(k)c(q) | \Psi_0 \rangle = \frac{1}{2\pi} \sum_{j,l=-\infty}^{+\infty} e^{ikj} e^{-iql} \langle \Psi_0 | c_j^\dagger c_l | \Psi_0 \rangle. \quad (30)$$

From the fermionic expression of the initial state $|\Psi_0\rangle$, we can show that

$$\begin{aligned} \langle \Psi_0 | c_j^\dagger c_l | \Psi_0 \rangle &= \langle \text{vac} | \dots \left(\cos \theta c_2 + \sin \theta \right) \left(\cos \theta c_1 + \sin \theta \right) \dots c_j^\dagger c_l | \text{vac} \rangle \\ &\quad \dots \left(\cos \theta c_1^\dagger + \sin \theta \right) \left(\cos \theta c_2^\dagger + \sin \theta \right) \dots | \text{vac} \rangle \\ &= \begin{cases} \cos^2(\theta), & \text{if } j = l, \\ \cos^2(\theta) \sin^2(\theta) [\sin^2(\theta) - \cos^2(\theta)]^{|j-l|-1}, & \text{if } j \neq l. \end{cases} \end{aligned} \quad (31)$$

Using Eqs. (30) and (31), we obtain Eq. (9) after a few algebraic manipulations.

C Derivation of Eq. (12)

In this appendix, we provide an analytical proof of the late-time algebraic decay $n \sim t^{-\chi}$ for the free fermionic system, where the critical exponent χ is given in Eq. (12).

From the Eq. (11) and by doing the change of variable $\varepsilon = k - k^*$ with $k^* = \pi - \phi$, we find

$$\begin{aligned} n &= \int_{-k^*}^{2\pi-k^*} \frac{d\varepsilon}{2\pi} \varrho_0(\varepsilon + k^*) e^{-2(1-\cos(\varepsilon))\kappa t} \\ &\underset{\kappa t \gg 1}{\approx} \int_{-\infty}^{+\infty} \frac{d\varepsilon}{2\pi} \left(\varrho_0(k^*) + \epsilon \frac{\partial \varrho_0}{\partial k} \Big|_{k=k^*} + \frac{\epsilon^2}{2} \frac{\partial^2 \varrho_0}{\partial k^2} \Big|_{k=k^*} \right) e^{-\varepsilon^2 \kappa t}. \end{aligned} \quad (32)$$

In the second line, we have performed a saddle point approximation around $\varepsilon = 0$. We then remark that,

$$\begin{aligned} \varrho_0(k^*) &\neq 0 \text{ if } \phi \neq 0 \text{ or } \theta = 0 \quad (\text{case 1}), \\ \varrho_0(k^*) = \frac{\partial \varrho_0}{\partial k} \Big|_{k=k^*} &= 0, \quad \frac{\partial^2 \varrho_0}{\partial k^2} \Big|_{k=k^*} \neq 0 \text{ if } \phi = 0 \text{ and } \theta \in \left(0, \frac{\pi}{2}\right) \quad (\text{case 2}). \end{aligned} \quad (33)$$

In the case 1, we consider only the dominant term of order $O(\varepsilon^0)$ in the Taylor expansion of $\varrho_0(\varepsilon + k^*)$, thus

$$n \approx \varrho_0(k^*) \int_{-\infty}^{+\infty} \frac{d\varepsilon}{2\pi} e^{-\varepsilon^2 \kappa t} = \varrho_0(k^*) \frac{1}{2\sqrt{\pi \kappa t}} \propto t^{-1/2}. \quad (34)$$

In the case 2, the dominant term in the Taylor expansion of $\varrho_0(\varepsilon + k^*)$ is of the order $O(\varepsilon^2)$, thus

$$n \approx \frac{\partial^2 \varrho_0}{\partial k^2} \Big|_{k=k^*} \int_{-\infty}^{+\infty} \frac{d\varepsilon}{2\pi} \frac{\varepsilon^2}{2} e^{-\varepsilon^2 \kappa t} = \frac{\partial^2 \varrho_0}{\partial k^2} \Big|_{k=k^*} \frac{1}{8\sqrt{\pi}(\kappa t)^{3/2}} \propto t^{-3/2}. \quad (35)$$

Finally, we mention that n can be written compactly in terms of the modified Bessel functions of the first kind $I_\alpha(x)$, in the cases $\theta = 0, \frac{\pi}{4}$. By using the substitution

$$e^{-2\kappa \cos(\phi+k)t} = \sum_{\alpha=-\infty}^{\infty} I_\alpha(-2\kappa t) e^{i\alpha(\phi+k)} \quad (36)$$

in Eq. (11), we can show that

$$n = \begin{cases} e^{-2\kappa t} I_0(2\kappa t), & \text{if } \theta = 0, \\ \frac{e^{-2\kappa t}}{2} [I_0(2\kappa t) - \cos(\phi) I_1(2\kappa t)], & \text{if } \theta = \frac{\pi}{4}. \end{cases} \quad (37)$$

The latter expressions are valid at any times. The asymptotic expansion of the modified Bessel functions reads

$$I_\alpha(x) = \frac{e^x}{\sqrt{2\pi x}} \left(1 - \frac{4\alpha^2 - 1}{8x} + O(x^{-2}) \right). \quad (38)$$

Thus, for $\kappa t \gg 1$, we obtain,

$$n \sim \begin{cases} \frac{1}{2\sqrt{\pi \kappa t}} \left(1 + \frac{1}{16\kappa t} \right), & \text{if } \theta = 0, \\ \frac{1}{4\sqrt{\pi \kappa t}} \left(1 - \cos \phi + \frac{1 + 3 \cos \phi}{16\kappa t} \right), & \text{if } \theta = \frac{\pi}{4}. \end{cases} \quad (39)$$

By keeping the first non-vanishing order in $(\kappa t)^{-1}$, we find again consistent results with Eq. (12).

D Derivation of Eq. (20)

In this appendix, we derive Eq. (20). We start from Eq. (19), and we compute independently $\langle L_j^\dagger L_j c^\dagger(k) c(k) \rangle$ and $\langle L_j^\dagger c^\dagger(k) c(k) L_j \rangle$; the expression of the operator L_j is given in Eq. (13).

First, we focus on $\langle L_j^\dagger L_j c^\dagger(k) c(k) \rangle$. For this term, the presence of a string operator in L_j 's expression does not play any role because

$$\begin{aligned} L_j^\dagger L_j &= \left(c_j^\dagger + e^{-i\phi} c_{j+1}^\dagger (-1)^{n_j} \right) \left(c_j + e^{i\phi} (-1)^{n_j} c_{j+1} \right) \\ &= c_j^\dagger c_j + e^{i\phi} c_j^\dagger (-1)^{n_j} c_{j+1} + e^{-i\phi} c_{j+1}^\dagger (-1)^{n_j} c_j + c_{j+1}^\dagger c_{j+1} \\ &= c_j^\dagger c_j + e^{i\phi} c_j^\dagger c_{j+1} + e^{-i\phi} c_{j+1}^\dagger c_j + c_{j+1}^\dagger c_{j+1}. \end{aligned} \quad (40)$$

By going in real space, we obtain

$$\begin{aligned} \langle L_j^\dagger L_j c^\dagger(k) c(k) \rangle &= \frac{1}{2\pi} \sum_{n,l=-\infty}^{+\infty} e^{ik(l-n)} \langle L_j^\dagger L_j c_l^\dagger c_n \rangle \\ &= \frac{1}{2\pi} \sum_{n,l=-\infty}^{+\infty} e^{ik(l-n)} \left(\langle c_j^\dagger c_j c_l^\dagger c_n \rangle + e^{i\phi} \langle c_j^\dagger c_{j+1} c_l^\dagger c_n \rangle \right. \\ &\quad \left. + e^{-i\phi} \langle c_{j+1}^\dagger c_j c_l^\dagger c_n \rangle + \langle c_{j+1}^\dagger c_{j+1} c_l^\dagger c_n \rangle \right). \end{aligned} \quad (41)$$

Using Eq. (41) and the following identities

$$\langle c_j^\dagger c_m c_l^\dagger c_n \rangle = \langle c_j^\dagger c_m \rangle \langle c_l^\dagger c_n \rangle + \langle c_j^\dagger c_n \rangle \langle c_m c_l^\dagger \rangle \quad (\text{Wick theorem}), \quad (42a)$$

$$\langle c_j^\dagger c_m \rangle = \frac{1}{2\pi} \int_0^{2\pi} dq \int_0^{2\pi} dp e^{-iqj} e^{ipm} \underbrace{\langle c^\dagger(q) c(p) \rangle}_{\delta(q-p)\varrho(q)} = \int_0^{2\pi} \frac{dq}{2\pi} e^{iq(m-j)} \varrho(q), \quad (42b)$$

$$\langle c_m c_j^\dagger \rangle = \frac{1}{2\pi} \int_0^{2\pi} dq \int_0^{2\pi} dp e^{-iqj} e^{ipm} \underbrace{\langle c(p) c^\dagger(q) \rangle}_{\delta(q-p)(1-\varrho(q))} = \int_0^{2\pi} \frac{dq}{2\pi} e^{iq(m-j)} (1 - \varrho(q)), \quad (42c)$$

$$\sum_{l=-\infty}^{\infty} e^{iKl} = 2\pi \sum_{m=-\infty}^{\infty} \delta(K - 2\pi m), \quad (42d)$$

we find

$$\begin{aligned} \pi \langle L_j^\dagger L_j c^\dagger(k) c(k) \rangle &= \int_0^{2\pi} \frac{dq}{2\pi} \varrho(q) (1 + 1 \cos(q + \phi)) \int_0^{2\pi} \frac{dp}{2\pi} \varrho(p) \left[\sum_l e^{i(k-p)l} \right] \left[\sum_n e^{i(p-k)n} \right] \\ &\quad + \varrho(k)(1 - \varrho(k))(1 + \cos(k + \phi)). \end{aligned} \quad (43)$$

The first term on the right-hand side of the latter expression diverges, however this divergence disappears when we subtract the contribution $\pi \langle L_j^\dagger c^\dagger(k) c(k) L_j \rangle$. Note that the Wick theorem could be applied here, because we assume that the system's density matrix is well approximated by the t-GGE (17) which is gaussian.

We now focus on the other term $\langle L_j^\dagger c^\dagger(k) c(k) L_j \rangle$ for which we have to take care of the string operators $(-1)^{n_j}$ and $(-1)^{N_{(-\infty, j-1)}}$. We have

$$\begin{aligned} \langle L_j^\dagger c^\dagger(k) c(k) L_j \rangle &= \\ &= \langle \left(c_j^\dagger + e^{-i\phi} c_{j+1}^\dagger (-1)^{n_j} \right) (-1)^{N_{(-\infty, j-1)}} c^\dagger(k) c(k) (-1)^{N_{(-\infty, j-1)}} \left(c_j + e^{i\phi} (-1)^{n_j} c_{j+1} \right) \rangle \\ &= \frac{1}{2\pi} \sum_{l,n=-\infty}^{\infty} e^{ik(l-n)} \langle \left(c_j^\dagger + e^{-i\phi} c_{j+1}^\dagger (-1)^{n_j} \right) (-1)^{N_{(-\infty, j-1)}} c_l^\dagger c_n \\ &\quad \times (-1)^{N_{(-\infty, j-1)}} \left(c_j + e^{i\phi} (-1)^{n_j} c_{j+1} \right) \rangle. \end{aligned} \quad (44)$$

The string operator induces sign functions, which we denote $s(l-j)$ and $\mu_{j,l}$:

$$(-1)^{N_{(-\infty, j-1)}} c_l^\dagger = s(l-j) c_l^\dagger (-1)^{N_{(-\infty, j-1)}}, \quad \text{with} \quad s(l-j) = \begin{cases} 1 & \text{if } l \geq j, \\ -1 & \text{if } l < j, \end{cases} \quad (45a)$$

$$(-1)^{n_j} c_l^\dagger = \mu_{j,l} c_l^\dagger (-1)^{n_j}, \quad c_l (-1)^{n_j} = \mu_{j,l} (-1)^{n_j} c_l, \quad \text{with} \quad \mu_{j,l} = \begin{cases} 1 & \text{if } l \neq j, \\ -1 & \text{if } l = j. \end{cases} \quad (45b)$$

Using Eqs. (44), (45), and that $\mu_{l,j} s(l-j) = -s(j-l)$, we obtain

$$\begin{aligned} \langle L_j^\dagger c^\dagger(k) c(k) L_j \rangle &= \frac{1}{2\pi} \sum_{l,n} e^{ik(l-n)} s(l-j) s(n-j) \left(\langle c_j^\dagger c_l^\dagger c_n c_j \rangle + \langle c_{j+1}^\dagger c_l^\dagger c_n c_{j+1} \rangle \right) \\ &\quad + \frac{1}{2\pi} \sum_{l,n} e^{ik(l-n)} s(j-l) s(j-n) \left(\langle c_j^\dagger c_l^\dagger c_n c_{j+1} \rangle e^{i\phi} + \langle c_{j+1}^\dagger c_l^\dagger c_n c_j \rangle e^{-i\phi} \right). \end{aligned} \quad (46)$$

From the Eqs. (46), (42b), (42c), the Wick theorem, and the identity

$$\forall K, \quad \sum_{l=-\infty}^{\infty} s(l-j) e^{iKl} = \frac{2e^{iKj}}{1 - e^{iK}} = \frac{ie^{iKj} e^{-iK/2}}{\sin(K/2)} = e^{iKj} (1 + i \cot(K/2)), \quad (47)$$

we obtain

$$\begin{aligned} \pi \langle L_j^\dagger c^\dagger(k) c(k) L_j \rangle &= A(k) + \int_0^{2\pi} \frac{dq}{2\pi} \varrho(q) (1 + \cos(q + \phi)) \\ &\quad \times \int_0^{2\pi} \frac{dp}{2\pi} \varrho(p) \left[\sum_l s(l-j) e^{i(k-p)l} \right] \left[s(n-j) \sum_n e^{i(p-k)n} \right], \end{aligned} \quad (48a)$$

$$\begin{aligned} \text{with } A(k) &:= - \int \frac{dq}{2\pi} \varrho(q) \int \frac{dp}{2\pi} \varrho(p) (1 + \cos(p + \phi)) \\ &\quad - \int \frac{dq}{2\pi} \varrho(q) \cot\left(\frac{k-q}{2}\right) \int \frac{dp}{2\pi} \varrho(p) \cot\left(\frac{k-p}{2}\right) (1 + \cos(p + \phi)) \\ &\quad + \int \frac{dq}{2\pi} \varrho(q) \int \frac{dp}{2\pi} \varrho(p) \sin(p + \phi) \left[\cot\left(\frac{k-q}{2}\right) - \cot\left(\frac{k-p}{2}\right) \right] \\ &= -2 \left(\int_0^{2\pi} \frac{dq}{2\pi} \varrho(q) \frac{\cos\left(\frac{q+\phi}{2}\right)}{\sin\left(\frac{k-q}{2}\right)} \right)^2. \end{aligned} \quad (48b)$$

Therefore,

$$\begin{aligned} & \pi \left[\langle L_j^\dagger L_j c^\dagger(k) c(k) \rangle - \langle L_j^\dagger c^\dagger(k) c(k) L_j \rangle \right] \\ &= \varrho(k) (1 - \varrho(k)) (1 + \cos(k + \phi)) - A(k) + \int \frac{dq}{2\pi} \varrho(q) (1 + \cos(q + \phi)) \oint \frac{dp}{2\pi} \varrho(p) Y(k - p), \end{aligned} \quad (49a)$$

$$\text{with } Y(K) := \left| \sum_{l=-\infty}^{\infty} e^{iKl} \right|^2 - \left| \sum_{l=-\infty}^{\infty} s(l) e^{iKl} \right|^2 = \sum_{m=-\infty}^{\infty} e^{iKm} \underbrace{\sum_{n=-\infty}^{\infty} (1 - s(m+n)s(n))}_{=2|m|}. \quad (49b)$$

By decomposing $\varrho(p)$ in Fourier modes, $\varrho(p) = \sum_m \varrho_m e^{imp}$, we can show that

$$\oint_0^{2\pi} dp \varrho(p) Y(k - p) = \oint_0^{2\pi} dp \frac{\varrho(k) - \varrho(p)}{\sin^2\left(\frac{k-p}{2}\right)}. \quad (50)$$

The latter expression, together with Eqs. (48b), (49a) and (19), leads to Eq. (20), or alternatively Eq. (21).

E Details on the numerical solution of Eq. (21)

To solve numerically Eq. (21), we discretize the momentum interval $[0, 2\pi]$ and use Runge–Kutta method. We also use the following relations between the circular Hilbert transform and the Fourier transform. By defining the Fourier transform and its inverse as

$$\mathcal{F}[f](n) = \int_0^{2\pi} f(x) e^{-inx} dx := \hat{f}_n, \quad \mathcal{F}^{-1}[g](x) = \sum_{n=-\infty}^{+\infty} g_n e^{inx}, \quad (51)$$

we have

$$\mathcal{F}[\mathcal{H}[f]](n) = -i \text{sgn}(n) \hat{f}_n \quad \text{where} \quad \text{sgn}(n) = \begin{cases} 1 & \text{if } n > 0 \\ 0 & \text{if } n = 0 \\ -1 & \text{if } n < 0, \end{cases} \quad (52)$$

$$\mathcal{F}[\mathcal{H}[f]'](n) = |n| \hat{f}_n. \quad (53)$$

Inverting Eqs. (52) and (53) provides an efficient method to compute a circular Hilbert transform or its derivative using fast Fourier transform.

F Details on the finite size numerical computation via quantum trajectories

In this appendix, we provide details about how to deal with a finite system size, with periodic boundary conditions (PBC), as it is the case in our quantum trajectory simulations. This is also the setup considered in Ref. [33, 36, 37].

For a finite system with lattice site $j \in \{1, 2, \dots, L\}$, the Jordan-Wigner transformation is defined as

$$c_j = (-1)^{N_{(1,j-1)}} S_j^-, \quad c_j^\dagger = (-1)^{N_{(1,j-1)}} S_j^+, \quad \text{with} \quad N_{(1,j)} = \sum_{l=1}^j n_l. \quad (54)$$

Importantly, we assume PBC for the spin operators, *i.e.* $S_{L+1}^+ = S_1^+$; this implies that the fermionic operators satisfy the boundary condition $c_{L+1}^\dagger = (-1)^{N_{(1,L)}-1} c_1^\dagger$. As a consequence, when going in Fourier space two different sets of momenta should be considered:

$$Q_p = \frac{2\pi}{L} \{1, 2, \dots, L\}, \quad Q_{ap} = \frac{2\pi}{L} \left\{ \frac{1}{2}, \frac{3}{2}, \dots, L - \frac{1}{2} \right\}. \quad (55)$$

Intuitively, the fermions satisfy PBC in the sector where the total number of particles is odd and anti PBC in the sector where the number of particles is even. In practice, the Fourier modes are expressed as

$$c_j^\dagger = \frac{1}{\sqrt{L}} \sum_{k \in Q_{ap}} e^{-ikj} c^\dagger(k) = \frac{1}{\sqrt{L}} \sum_{k \in Q_p} e^{-ikj} c^\dagger(k), \quad \forall k \in Q, \quad c^\dagger(k) = \frac{1}{\sqrt{L}} \sum_{j=1}^L e^{ikj} c_j^\dagger, \quad (56)$$

where $Q := Q_{ap} \cup Q_p$, and the Hamiltonian is

$$H = -\frac{J}{2} \sum_{j=1}^L \left(S_{j+1}^+ S_j^- + S_j^+ S_{j+1}^- \right) = \sum_{k \in Q_{ap}} \epsilon_k P_+ c^\dagger(k) c(k) + \sum_{k \in Q_p} \epsilon_k P_- c^\dagger(k) c(k), \quad (57)$$

with

$$\epsilon_k = -J \cos k, \quad \text{and} \quad P_\pm = \frac{1}{2} (1 \pm (-1)^{N_{(1,L)}}). \quad (58)$$

The finite system size rapidity distribution is defined as

$$\forall k \in Q_{ap}, \quad \varrho_{ap}(k) = \langle P_+ c^\dagger(k) c(k) \rangle, \quad \forall k \in Q_p, \quad \varrho_p(k) = \langle P_- c^\dagger(k) c(k) \rangle, \quad (59)$$

$$\forall n \in \{1, \dots, L\}, \quad \tilde{\varrho}(2\pi(n-1/4)/L) = \varrho_{ap}(2\pi(n-1/2)/L) + \varrho_p(2\pi n/L). \quad (60)$$

The crosses in Fig. 3 correspond to the distribution $\tilde{\varrho}$, computed using quantum trajectories for $L = 14$. Empirically, we found that $\tilde{\varrho}$ is a good proxy for the comparison with the t-GGE results.

References

- [1] M. Nagy, Z. Ákos, D. Biro and T. Vicsek, *Hierarchical group dynamics in pigeon flocks*, *Nature* **464**(7290), 890 (2010), doi:[10.1038/nature08891](https://doi.org/10.1038/nature08891).
- [2] T. H. Tan, A. Mietke, J. Li, Y. Chen, H. Higinbotham, P. J. Foster, S. Gokhale, J. Dunkel and N. Fakhri, *Odd dynamics of living chiral crystals*, *Nature* **607**(7918), 287 (2022), doi:[10.1038/s41586-022-04889-6](https://doi.org/10.1038/s41586-022-04889-6).
- [3] A. Dinelli, J. O’Byrne, A. Curatolo, Y. Zhao, P. Sollich and J. Tailleur, *Non-reciprocity across scales in active mixtures*, *Nature Communications* **14**(1), 7035 (2023), doi:[10.1038/s41467-023-42713-5](https://doi.org/10.1038/s41467-023-42713-5).
- [4] N. Uchida and R. Golestanian, *Synchronization and Collective Dynamics in a Carpet of Microfluidic Rotors*, *Phys. Rev. Lett.* **104**, 178103 (2010), doi:[10.1103/PhysRevLett.104.178103](https://doi.org/10.1103/PhysRevLett.104.178103).
- [5] M. Brandenbourger, X. Locsin, E. Lerner and C. Coulais, *Non-reciprocal robotic metamaterials*, *Nature Communications* **10**(1), 4608 (2019), doi:[10.1038/s41467-019-12599-3](https://doi.org/10.1038/s41467-019-12599-3).

[6] M. Fruchart, R. Hanai, P. B. Littlewood and V. Vitelli, *Non-reciprocal phase transitions*, Nature **592**(7854), 363 (2021), doi:[10.1038/s41586-021-03375-9](https://doi.org/10.1038/s41586-021-03375-9).

[7] Y. Avni, M. Fruchart, D. Martin, D. Seara and V. Vitelli, *Dynamical phase transitions in the nonreciprocal Ising model*, Phys. Rev. E **111**, 034124 (2025), doi:[10.1103/PhysRevE.111.034124](https://doi.org/10.1103/PhysRevE.111.034124).

[8] T. Vicsek and A. Zafeiris, *Collective motion*, Physics Reports **517**(3–4), 71–140 (2012), doi:[10.1016/j.physrep.2012.03.004](https://doi.org/10.1016/j.physrep.2012.03.004).

[9] M. Fruchart, C. Scheibner and V. Vitelli, *Odd Viscosity and Odd Elasticity*, Annual Review of Condensed Matter Physics **14**(1), 471–510 (2023), doi:[10.1146/annurev-connatphys-040821-125506](https://doi.org/10.1146/annurev-connatphys-040821-125506).

[10] M. K. Johnsrud and R. Golestanian, *Fluctuation dissipation relations for active field theories*, Phys. Rev. Res. **7**, L032053 (2025), doi:[10.1103/xx4z-lj5c](https://doi.org/10.1103/xx4z-lj5c).

[11] Y. Ashida, Z. Gong and M. Ueda, *Non-Hermitian physics*, Advances in Physics **69**(3), 249–435 (2020), doi:[10.1080/00018732.2021.1876991](https://doi.org/10.1080/00018732.2021.1876991).

[12] N. Hatano and D. R. Nelson, *Localization Transitions in Non-Hermitian Quantum Mechanics*, Phys. Rev. Lett. **77**, 570 (1996), doi:[10.1103/PhysRevLett.77.570](https://doi.org/10.1103/PhysRevLett.77.570).

[13] N. Hatano and D. R. Nelson, *Vortex pinning and non-Hermitian quantum mechanics*, Phys. Rev. B **56**, 8651 (1997), doi:[10.1103/PhysRevB.56.8651](https://doi.org/10.1103/PhysRevB.56.8651).

[14] Z. Gong, Y. Ashida, K. Kawabata, K. Takasan, S. Higashikawa and M. Ueda, *Topological phases of non-hermitian systems*, Phys. Rev. X **8**, 031079 (2018), doi:[10.1103/PhysRevX.8.031079](https://doi.org/10.1103/PhysRevX.8.031079).

[15] N. Okuma, K. Kawabata, K. Shiozaki and M. Sato, *Topological Origin of Non-Hermitian Skin Effects*, Phys. Rev. Lett. **124**, 086801 (2020), doi:[10.1103/PhysRevLett.124.086801](https://doi.org/10.1103/PhysRevLett.124.086801).

[16] A. Metelmann and A. A. Clerk, *Nonreciprocal Photon Transmission and Amplification via Reservoir Engineering*, Phys. Rev. X **5**, 021025 (2015), doi:[10.1103/PhysRevX.5.021025](https://doi.org/10.1103/PhysRevX.5.021025).

[17] A. Metelmann and A. A. Clerk, *Nonreciprocal quantum interactions and devices via autonomous feedforward*, Phys. Rev. A **95**, 013837 (2017), doi:[10.1103/PhysRevA.95.013837](https://doi.org/10.1103/PhysRevA.95.013837).

[18] A. A. Clerk, *Introduction to quantum non-reciprocal interactions: from non-Hermitian Hamiltonians to quantum master equations and quantum feedforward schemes*, SciPost Phys. Lect. Notes p. 44 (2022), doi:[10.21468/SciPostPhysLectNotes.44](https://doi.org/10.21468/SciPostPhysLectNotes.44).

[19] R. Fazio, J. Keeling, L. Mazza and M. Schirò, *Many-body open quantum systems*, SciPost Phys. Lect. Notes p. 99 (2025), doi:[10.21468/SciPostPhysLectNotes.99](https://doi.org/10.21468/SciPostPhysLectNotes.99).

[20] A. McDonald, R. Hanai and A. A. Clerk, *Nonequilibrium stationary states of quantum non-Hermitian lattice models*, Phys. Rev. B **105**, 064302 (2022), doi:[10.1103/PhysRevB.105.064302](https://doi.org/10.1103/PhysRevB.105.064302).

[21] M. Keck, D. Rossini and R. Fazio, *Persistent currents by reservoir engineering*, Phys. Rev. A **98**, 053812 (2018), doi:[10.1103/PhysRevA.98.053812](https://doi.org/10.1103/PhysRevA.98.053812).

[22] F. Song, S. Yao and Z. Wang, *Non-Hermitian Skin Effect and Chiral Damping in Open Quantum Systems*, Phys. Rev. Lett. **123**, 170401 (2019), doi:[10.1103/PhysRevLett.123.170401](https://doi.org/10.1103/PhysRevLett.123.170401).

[23] D. Porras and S. Fernández-Lorenzo, *Topological Amplification in Photonic Lattices*, Phys. Rev. Lett. **122**, 143901 (2019), doi:[10.1103/PhysRevLett.122.143901](https://doi.org/10.1103/PhysRevLett.122.143901).

[24] C. C. Wanjura, M. Brunelli and A. Nunnenkamp, *Topological framework for directional amplification in driven-dissipative cavity arrays*, Nature Communications **11**, 3149 (2020), doi:[10.1038/s41467-020-16863-9](https://doi.org/10.1038/s41467-020-16863-9).

[25] M. Brunelli, C. C. Wanjura and A. Nunnenkamp, *Restoration of the non-Hermitian bulk-boundary correspondence via topological amplification*, SciPost Phys. **15**, 173 (2023), doi:[10.21468/SciPostPhys.15.4.173](https://doi.org/10.21468/SciPostPhys.15.4.173).

[26] P. Brighi and A. Nunnenkamp, *Nonreciprocal dynamics and the non-Hermitian skin effect of repulsively bound pairs*, Phys. Rev. A **110**, L020201 (2024), doi:[10.1103/PhysRevA.110.L020201](https://doi.org/10.1103/PhysRevA.110.L020201).

[27] S. E. Begg and R. Hanai, *Quantum Criticality in Open Quantum Spin Chains with Nonreciprocity*, Phys. Rev. Lett. **132**, 120401 (2024), doi:[10.1103/PhysRevLett.132.120401](https://doi.org/10.1103/PhysRevLett.132.120401).

[28] R. Belyansky, C. Weis, R. Hanai, P. B. Littlewood and A. A. Clerk, *Phase Transitions in Nonreciprocal Driven-Dissipative Condensates*, Phys. Rev. Lett. **135**, 123401 (2025), doi:[10.1103/gphr-d1bc](https://doi.org/10.1103/gphr-d1bc).

[29] R. D. Soares, M. Brunelli and M. Schirò, *Dissipative phase transition of interacting non-reciprocal fermions* (2025), [2505.15711](https://arxiv.org/abs/2505.15711).

[30] F. Lange, Z. Lenarčič and A. Rosch, *Time-dependent generalized Gibbs ensembles in open quantum systems*, Physical Review B **97**(16) (2018), doi:[10.1103/physrevb.97.165138](https://doi.org/10.1103/physrevb.97.165138).

[31] L. Vidmar and M. Rigol, *Generalized Gibbs ensemble in integrable lattice models*, Journal of Statistical Mechanics: Theory and Experiment p. 064007 (2016), doi:[10.1088/1742-5468/2016/06/064007](https://doi.org/10.1088/1742-5468/2016/06/064007).

[32] F. H. L. Essler and M. Fagotti, *Quench dynamics and relaxation in isolated integrable quantum spin chains*, Journal of Statistical Mechanics: Theory and Experiment **2016**(6), 064002 (2016), doi:[10.1088/1742-5468/2016/06/064002](https://doi.org/10.1088/1742-5468/2016/06/064002).

[33] I. Bouchoule, B. Doyon and J. Dubail, *The effect of atom losses on the distribution of rapidities in the one-dimensional Bose gas*, SciPost Phys. **9**, 044 (2020), doi:[10.21468/SciPostPhys.9.4.044](https://doi.org/10.21468/SciPostPhys.9.4.044).

[34] D. Rossini, A. Ghermaoui, M. B. Aguilera, R. Vatré, R. Bouganne, J. Beugnon, F. Gerbier and L. Mazza, *Strong correlations in lossy one-dimensional quantum gases: From the quantum Zeno effect to the generalized Gibbs ensemble*, Phys. Rev. A **103**, L060201 (2021), doi:[10.1103/PhysRevA.103.L060201](https://doi.org/10.1103/PhysRevA.103.L060201).

[35] L. Rosso, A. Biella and L. Mazza, *The one-dimensional Bose gas with strong two-body losses: the effect of the harmonic confinement*, SciPost Phys. **12**, 044 (2022), doi:[10.21468/SciPostPhys.12.1.044](https://doi.org/10.21468/SciPostPhys.12.1.044).

[36] F. Riggio, L. Rosso, D. Karevski and J. Dubail, *Effects of atom losses on a one-dimensional lattice gas of hard-core bosons*, Physical Review A **109**(2) (2024), doi:[10.1103/physreva.109.023311](https://doi.org/10.1103/physreva.109.023311).

[37] L. Lumia, G. Aupetit-Diallo, J. Dubail and M. Collura, *Accuracy of a time-dependent generalized Gibbs ensemble approach under weak dissipation*, Phys. Rev. A **112**, 012206 (2025), doi:[10.1103/x9c1-hyxh](https://doi.org/10.1103/x9c1-hyxh).

[38] G. Perfetto, F. Carollo, J. P. Garrahan and I. Lesanovsky, *Reaction-Limited Quantum Reaction-Diffusion Dynamics*, Physical Review Letters **130**(21) (2023), doi:[10.1103/physrevlett.130.210402](https://doi.org/10.1103/physrevlett.130.210402).

[39] H. Lehr, I. Lesanovsky and G. Perfetto, *Reaction-diffusion dynamics of the weakly dissipative Fermi gas*, New Journal of Physics **27**(8), 084602 (2025), doi:[10.1088/1367-2630/adef70](https://doi.org/10.1088/1367-2630/adef70).

[40] I. Ulčakar and Z. Lenarčič, *Generalized Gibbs ensembles in weakly interacting dissipative systems and digital quantum computers*, SciPost Phys. **19**, 068 (2025), doi:[10.21468/SciPostPhys.19.3.068](https://doi.org/10.21468/SciPostPhys.19.3.068).

[41] F. Reiter, F. Lange, S. Jain, M. Grau, J. P. Home and Z. Lenarčič, *Engineering generalized Gibbs ensembles with trapped ions*, Phys. Rev. Res. **3**, 033142 (2021), doi:[10.1103/PhysRevResearch.3.033142](https://doi.org/10.1103/PhysRevResearch.3.033142).

[42] Z. Cai and T. Barthel, *Algebraic versus Exponential Decoherence in Dissipative Many-Particle Systems*, Phys. Rev. Lett. **111**, 150403 (2013), doi:[10.1103/PhysRevLett.111.150403](https://doi.org/10.1103/PhysRevLett.111.150403).

[43] D. Poletti, J.-S. Bernier, A. Georges and C. Kollath, *Interaction-Induced Impeding of Decoherence and Anomalous Diffusion*, Phys. Rev. Lett. **109**, 045302 (2012), doi:[10.1103/PhysRevLett.109.045302](https://doi.org/10.1103/PhysRevLett.109.045302).

[44] D. Poletti, P. Barmettler, A. Georges and C. Kollath, *Emergence of Glasslike Dynamics for Dissipative and Strongly Interacting Bosons*, Physical Review Letters **111**(19) (2013), doi:[10.1103/physrevlett.111.195301](https://doi.org/10.1103/physrevlett.111.195301).

[45] A. Marché, H. Yoshida, A. Nardin, H. Katsura and L. Mazza, *Universality and two-body losses: Lessons from the effective non-Hermitian dynamics of two particles*, Phys. Rev. A **110**, 033321 (2024), doi:[10.1103/PhysRevA.110.033321](https://doi.org/10.1103/PhysRevA.110.033321).

[46] A. Pocklington and A. A. Clerk, *Efficient Simulation of Nontrivial Dissipative Spin Chains via Stochastic Unraveling*, PRX Quantum **6**, 030349 (2025), doi:[10.1103/vptq-xy6h](https://doi.org/10.1103/vptq-xy6h).

[47] F. W. King, *The Hilbert transform of periodic functions*, p. 288–330, Encyclopedia of Mathematics and its Applications. Cambridge University Press (2009).

[48] J. N. Pandey, *The Hilbert transform of periodic distributions*, Integral Transforms and Special Functions **5**(1-2), 117 (1997), doi:[10.1080/10652469708819129](https://doi.org/10.1080/10652469708819129), <https://doi.org/10.1080/10652469708819129>.

[49] J. Johansson, P. Nation and F. Nori, *QuTiP: An open-source Python framework for the dynamics of open quantum systems*, Computer Physics Communications **183**(8), 1760 (2012), doi:<https://doi.org/10.1016/j.cpc.2012.02.021>.

[50] J. Johansson, P. Nation and F. Nori, *QuTiP 2: A Python framework for the dynamics of open quantum systems*, Computer Physics Communications **184**(4), 1234 (2013), doi:<https://doi.org/10.1016/j.cpc.2012.11.019>.